Available online at www.sciencedirect.com
ScienceDirect
Earth and Planetary Science Letters 257 (2007) 290–298
EPSL
www.elsevier.com/locate/epsl

Quantifying trace element disequilibria in mantle xenoliths and abyssal peridotites

Arnaud Agranier *, Cin-Ty Aeolus Lee

Department of Earth Science, MS-126, Rice University, 6100 Main St., Houston, TX 77005, United States

Received 25 January 2007; received in revised form 27 February 2007; accepted 27 February 2007
Available online 6 March 2007
Editor: R.W. Carlson

Abstract

We apply a tool based on element distribution between orthopyroxene and clinopyroxene for quantifying rare earth element (REE) disequilibria in ultramafic rocks in the subsolidus state. We present case studies of the REE contents of mineral cores in mantle xenoliths and abyssal peridotites using in situ analytical tools. Even when only mineral cores are measured (to avoid enriched rims), equilibrium is not always achieved on the mineral scale. Mineral cores in mantle xenoliths are closer to equilibrium than those in abyssal peridotites even though mantle xenoliths are known to be light REE-contaminated from the host lava. In the case of the abyssal peridotites, 13 out of 14 are out of equilibrium with the least metasomatized most in disequilibrium and the most metasomatized closest to equilibrium. We discuss hypotheses for these observations, but regardless of what caused the disequilibria, this tool allows one to "see through" the effects of secondary processes, such as infiltration by fluid inclusions via cracks and diffusive exchange between minerals and melts/fluids along grain boundaries. The ease of making in situ REE measurements makes this tool formidable in identifying different generations of clinopyroxenes in ultramafic lithologies. Such data will complement the interpretation of isotopic and petrographic studies of continental and oceanic lithospheric mantle.

Keywords: rare earth elements; disequilibrium; LA-ICP-MS; partition coefficient; peridotite; xenolith; Dish Hill; abyssal peridotite

1. Introduction

There has been a recent increase in the number of studies on the isotopic signatures of mantle peridotites in the form of xenoliths, obducted massifs, and exhumed mantle blocks (e.g., abyssal peridotites in slow spreading ridges). In part, this has been motivated by an interest in the physical and chemical origins and evolution of oceanic and continental lithospheric mantle, but it has also been facilitated by the growing availability of multiple-collector inductively coupled plasma mass spectrometers [1], which have eased the measurements of samples with low quantities of trace elements, such as ultramafic rocks.

Of particular concern are radiogenic isotope ratios, such as $^{143}Nd/^{144}Nd$, $^{176}Hf/^{177}Hf$, $^{187}Os/^{188}Os$, $^{207}Pb/^{204}Pb$, $^{206}Pb/^{204}Pb$, $^{208}Pb/^{204}Pb$, and $^{87}Sr/^{86}Sr$. These isotopes are now so widely used to determine lithospheric formation ages or the timing and nature of metasomatic events that they have become standard, if not required, tools in many geochemical studies of the lithosphere [2–4]. However, what has not kept up with the proliferation of isotopic studies is the foundation for

* Corresponding author. Tel.: +1 713 348 4675; fax: +1 713 348 5214.
E-mail address: arnaud@rice.edu (A. Agranier).

0012-821X/$ - see front matter © 2007 Elsevier B.V. All rights reserved.
doi:10.1016/j.epsl.2007.02.041

interpreting whether mantle peridotites are in equilibrium with respect to the trace elements relevant to these isotopic systems.

For example, mantle xenoliths are often contaminated on grain boundaries by infiltration from the host lava or recent mantle metasomatism occurring just before eruption, and such contamination could also work its way into mineral interiors by solid-state diffusion or as fluid inclusions along cracks [5,6]. Seeing through these "secondary" processes is clearly necessary to constrain the pre-eruptive compositions of a peridotite xenolith. Similarly, abyssal peridotites, which sample the cold upper part of the oceanic lithospheric mantle, have often experienced precipitation of secondary minerals, such as magmatic clinopyroxene, due to infiltration and subsequent freezing in of small amounts of magma. How can these secondary pyroxenes be distinguished from primary pyroxenes? While these secondary pyroxenes can often be identified on the basis of texture and major element chemistry, this is not always the case. Secondary pyroxenes could have re-equilibrated in terms of major elements (e.g., Ca, Fe, Mg), but re-equilibration of trace elements, such as the rare earth elements and Hf, may lag substantially due to their much slower diffusivities ([7]).

Attempts to "see through" recent metasomatism or contamination have typically relied on measuring clinopyroxene grains, whose rims or surfaces have been removed by acid leaching or physical abrasion [8]. The limitations of this approach are that there is no easy way to develop a systematic mineral cleansing procedure that consistently rids minerals of metasomatized rims because the extent of disequilibrium varies from sample to sample. Moreover, these surface-cleansing procedures will not remove fluid inclusions trapped in the interior of a mineral. Additional approaches, such as establishing internal isochrons or checking for major-element equilibria, are also not ideal. In many mantle peridotites, only clinopyroxene and garnet have sufficiently high amounts of trace elements for isotopic measurements (olivine and orthopyroxene are poor in trace elements), giving at best two point isochrons, which are effectively meaningless.

As a step towards resolving these problems, we developed in an earlier manuscript a potentially rapid and efficient tool for identifying mineral assemblages that are in rare earth element equilibrium [9]. These principles are now applied here to natural samples using in situ trace element data based on in situ analytical techniques (laser ablation ICP-MS and SIMS). The utility of this filtering tool is demonstrated in a case study of peridotite xenoliths and abyssal peridotites. We show that this new tool provides a framework for categorizing different generations of metasomatic events, opening up avenues for further research and re-interpretation of previous studies.

2. Subsolidus partitioning of rare earth elements

In a previous study [9], we showed that the lattice strain model of Blundy and Wood [10] for equilibrium trace element partitioning between mineral and melt could be modified for subsolidus partitioning between olivine and pyroxene. For example, equilibrium partitioning of a trivalent trace element, such as a rare earth element (REE), between orthopyroxene and clinopyroxene $D_i^{opx/cpx}$ is related to its cation radius r_i in 8-fold coordination as follows:

$$D_i^{opx/cpx} = D_{Lu}^{opx/cpx}\exp\left(\frac{-4\pi N_A}{RT}\left[\frac{1}{2}(r_{Lu}^2 - r_i^2) \times (E_{opx}r_o^{opx} - E_{cpx}r_o^{cpx}) + \frac{1}{3}(r_i^3 - r_{Lu}^3) \times (E_{opx} - E_{cpx})\right]\right) \quad (1)$$

where $D_{Lu}^{opx/cpx}$ is the partition coefficient of a reference REE (taken here to be Lu), π is pi, N_A is Avogadro's number, T is temperature (in Kelvin), R is the gas constant, r_{Lu} is the 8-fold cation radius of Lu, r_o^{opx} and r_o^{cpx} are the optimum site radii of a trivalent cation in orthopyroxene and clinopyroxene, and E_{opx} and E_{cpx} are the Young's moduli of cation site for orthopyroxene and clinopyroxene. The partition coefficient of an element between orthopyroxene and clinopyroxene, $D_i^{opx/cpx}$, depends on temperature, pressure and the major-element composition of the mineral, but all these dependencies, to first order, are subsumed in the pre-exponential term in Eq. (1), e.g., $D_{Lu}^{opx/cpx}$ [10–13]. Provided $D_{Lu}^{opx/cpx}$ is independently known for a given mineral pair, the equilibrium partition coefficients of the remaining REEs are predicted precisely. We have chosen $D_{Lu}^{opx/cpx}$ as our reference element because Lu, being the heaviest REE, is mildly incompatible during melting, contrasting with the light REEs (LREEs), which are highly incompatible during melting. Therefore, in peridotites, Lu is least likely of all the REEs to be disturbed by metasomatism and most likely to remain in equilibrium between minerals [14]. An analogous formulation can be constructed for olivine/clinopyroxene partitioning.

Equilibrium and disequilibrium REE distribution between orthopyroxene, clinopyroxene, and olivine is shown schematically in Fig. 1. At equilibrium, there is a

negative correlation between Opx/Cpx ($D_i^{opx/cpx}$) and Ol/Cpx ($D_i^{ol/cpx}$) REE ratios when plotted against cationic radii. Increases in temperature (following the work of [15]) result in an increase in Opx/Cpx and Ol/Cpx partition coefficients (Fig. 1). If there has been recent introduction of a LREE-enriched contaminant or metasomatic component and if equilibrium between Opx/Cpx and Ol/Cpx pairs is not re-established, the trend of Opx/Cpx and Ol/Cpx REE ratios versus cationic radii will deviate from the equilibrium curves and yield U-shaped curves (Fig. 1A). Deviations from equilibrium are most pronounced in the LREEs because the proportion of LREE contamination is greatest. This is because almost all possible contaminants are melts or fluids and hence they will be most enriched in highly incompatibles, such as the LREEs, and only slightly enriched in the moderately incompatibles, such as the HREEs. Indeed, re-examination of previously published mineral REE data from mantle xenoliths in this context reveals that unleached mineral grains plot in the disequilibrium field while leached mineral grains tend to lie closer to or on the equilibrium curves.

To summarize, equilibrium partitioning of REEs between orthopyroxene and clinopyroxene (as well as

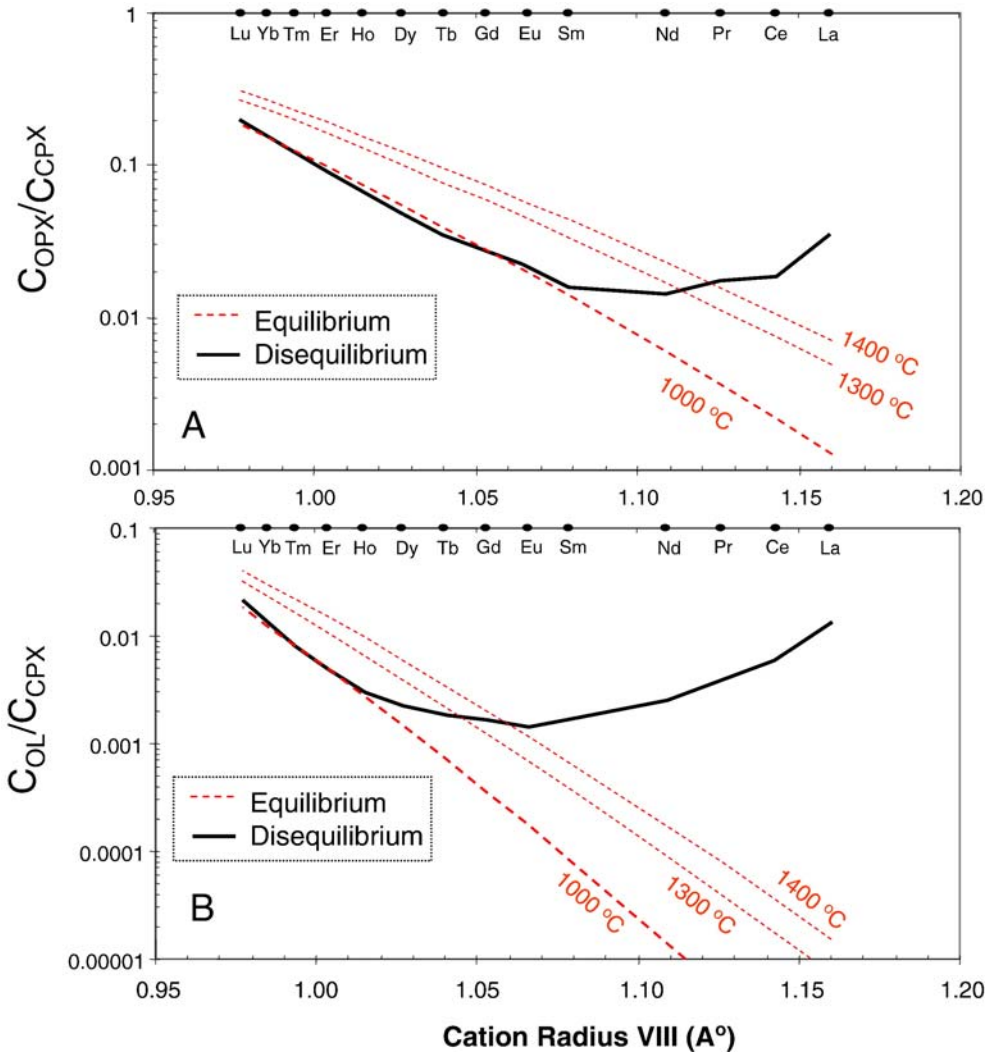

Fig. 1. Diagram shows distribution of a rare earth element (REE) concentration between A) orthopyroxene (opx) and clinopyroxene (cpx) and B) between olivine (ol) and cpx as a function of trivalent cationic radius in VIII-fold coordination ($A°$). Red dashed lines show how REEs are distributed between mineral phases at equilibrium for three different temperatures. Black solid line in each panel shows one example of Opx/Cpx and Ol/Cpx pairs that have been recently re-enriched by a light REE-enriched melt or contaminant without re-establishment of equilibrium. (For interpretation of the references to colour in this figure legend, the reader is referred to the web version of this article.)

between olivine and clinopyroxene) should decrease monotonically with increasing cation radius. This equilibrium relationship is independent of what the REE abundance pattern of individual clinopyroxene grains look like. Deviations from equilibrium are generally manifested by apparent increases in the ratio of LREEs between orthopyroxene and clinopyroxene, resulting in concave-upward patterns on plots of $D_i^{opx/cpx}$ versus cation radius.

2.1. Applications to mineral cores in mantle xenoliths and abyssal peridotites

To illustrate the utility of Eq. (1) in quantifying REE disequilibria, we present here case studies of REE distribution between orthopyroxene and clinopyroxene in mantle xenoliths from Dish Hill in southeastern California (subcontinental lithospheric mantle) and abyssal peridotites from the Gakkel Ridge (oceanic lithospheric mantle at a ultraslow-spreading ridge). The xenolith study represents new laser ablation ICP-MS measurements on mineral cores from xenoliths collected by the second author during his dissertation 7 years ago [16]. The abyssal peridotite data are taken directly from published secondary ionization mass spectrometry measurements on mineral cores [17]. Last "equilibration" temperatures recorded by Ca exchange between clinopyroxenes and orthopyroxenes in the Dish Hill xenoliths and Gakkel ridge abyssal peridotites fall between 900 and 1100 °C.

3. Analytical techniques

3.1. Major elements

Othopyroxene, clinopyroxene, spinel and olivine crystals were handpicked from coarsely crushed samples, impregnated into epoxy resin and polished. No obvious evidence of inclusion could be detected during grain optical inspections. Major elements (Table 1) were measured using the Cameca MBX electron Microprobe at Harvard University following analytical protocol described in Lee et al. [18].

3.2. Trace elements

LA-ICP-MS was used to measure rare earth elements as well as some of the major elements (Mg, Ca, Fe) (Table 2). Grains analyzed are the same as in the microprobe study. The ICP-MS used in this work is a ThermoFinnigan Element 2 at Rice University operated in low resolution mode ($m/\Delta m = 300$) for about 100 cycles depending on the thickness of samples. The ablation setup utilizes a 213 nm wavelength laser from NewWave. The power output of the laser is approximately 60 W, with pulsing set at 20 Hz and a spot size of 55 μm. Transmission was typically estimated at about 10^5 cps/ppm of La in the BHVO-2 glass standard. Gas blanks were systematically checked by running 20 cycles of measurements before igniting the laser. They remained typically lower than 60 cps for rare earth elements. Drift in ablation yield as well as matrix effects

Table 1
Major elements (weight %)

Sample name	Mineral identification	SiO_2	TiO_2	Al_2O_3	FeO	MgO	CaO	Na_2O	NiO	Cr_2O_3	MnO	Total
Dish Hill 120	cpx	50.5	0.45	8.4	3.4	14.8	20.3	1.0		0.30	0.12	99.2
	opx	53.3	0.08	7.0	7.0	31.5	0.7	0.08		0.2	0.2	100.1
Dish Hill 25	ol	40.1	0.02	0.03	9.1	48.3	0.07		0.4	–	0.11	98.1
	cpx	51.9	0.4	6.1	2.7	15.4	20.6	1.3		0.8	0.10	99.2
	opx	55.4	0.06	4.1	5.9	33.6	0.6	0.09		0.3	0.15	100.2
Dish Hill 9	ol	39.8	0.02	0.04	9.7	48.4	0.10		0.3	0.00	0.12	98.4
	cpx	50.9	0.5	7.2	3.6	15.9	18.9	1.4		0.8	0.11	99.2
	opx	54.1	0.11	5.3	6.3	32.2	1.0	0.14		0.4	0.11	99.7
Dish Hill 32	ol	39.7	0.02	0.01	12.1	46.3	0.1		0.4	0.02	0.20	98.8
	cpx	52.8	0.08	4.5	3.8	16.1	20.0	1.2		1.0	0.14	99.7
	opx	55.2	0.06	3.2	7.8	32.0	0.9	0.11		0.5	0.22	100.2
Dish Hill 18	ol	40.2	0.03	0.02	10.3	48.0	0.07		0.4	0.00	0.14	99.2
	ol	40.0	0.01	0.01	10.1	47.8	0.11		0.3	0.01	0.14	98.6
	cpx	50.7	0.7	7.3	3.4	15.1	19.7	1.5		0.6	0.07	98.9
	opx	54.6	0.09	4.8	6.7	32.4	0.8	0.11		0.3	0.11	99.8
Dish Hill 6	ol	39.9	0.03	0.02	11.4	46.8	0.10		0.4	0.01	0.18	98.8
	cpx	51.3	0.3	6.5	3.8	15.3	19.6	1.4		0.9	0.13	99.3
	opx	54.1	0.10	4.7	7.3	32.0	0.9	0.10		0.4	0.18	99.8
	sp	0.1	0.13	53.6	14.3	19.3	0.01		0.3	12.0	0.10	99.8

Electron microprobe data. opx = orthopyroxene, cpx = clinopyroxene, ol = olivine, sp = spinel.

Table 2
Rare earth elements (ppm)

Sample name	Identification #	Mineral identification	Assumed MgO content (%)	La	Ce	Pr	Nd	Sm	Eu	Tb	Gd	Dy	Ho	Er	Yb	Lu
BCR2		Glass	2.10	24	48	5.9	27	6.0	1.8	0.9	6.1	5.7	1.2	3.1	3.1	0.44
BHVO2		Glass	4.27	18	45	5.5	25	5.9	2.0	0.8	5.7	5.0	1.0	2.4	1.9	0.27
Dish Hill 120	DH120 2	opx	19.0	0.016	0.07	0.009	0.04	0.01	0.004	0.005	0.02	0.05	0.02	0.10	0.16	0.04
	DH120 3	ol	29.1	0.002	0.002	0.0004	0.005	–	0.001	–	0.01	0.01	0.002	0.01	0.03	0.01
	DH120 4	ol	29.1	0.06	0.11	0.01	0.04	0.01	0.002	0.002	0.01	0.01	0.01	0.01	0.03	0.01
	DH120 5	cpx	8.9	6	14	1.3	3.6	0.5	0.2	0.1	0.5	0.7	0.2	0.7	0.7	0.11
	DH120 6	cpx	8.9	6	14	1.1	3.1	0.4	0.1	0.1	0.4	0.7	0.2	0.7	0.7	0.10
	DH120 1	ol	29.1	0.01	0.04	0.002	0.01	–	0.002	–	0.01	0.01	0.01	0.01	0.02	0.01
	DH120 2	opx	19.0	0.02	0.08	0.01	0.05	0.01	0.01	0.01	0.03	0.07	0.02	0.11	0.19	0.04
Dish Hill 25	DH25 1	ol	29.1	0.002	0.002	0.0005	0.002	0.005	0.001	0.001	0.004	0.01	0.002	0.01	0.02	0.01
	DH25 2	ol	29.1	0.001	0.001	0.001	0.004	–	–	0.001	0.002	0.01	0.001	0.01	0.02	0.01
	DH25 3	opx	20.2	0.003	0.030	0.0009	0.01	–	0.01	0.01	0.02	0.07	0.03	0.11	0.21	0.05
	DH25 4	opx	20.2	0.001	0.004	0.001	0.008	0.002	0.004	0.007	0.030	0.08	0.03	0.11	0.20	0.04
	DH25 5	cpx	9.3	0.6	0.9	0.13	0.8	0.4	0.2	0.2	0.8	1.4	0.4	1.3	1.1	0.19
	DH25 6	cpx	9.3	0.57	0.86	0.13	0.7	0.4	0.2	0.2	0.8	1.4	0.4	1.2	1.1	0.17
Dish Hill 9	DH9 1	ol	29.1	0.001	0.001	0.001	0.005	–	0.001	0.001	0.004	0.011	0.004	0.02	0.04	0.01
	DH9 2	ol	29.1	0.002	–	0.001	0.01	0.01	0.002	–	0.004	0.010	0.004	0.01	0.04	0.01
	DH9 3	ol	29.1	0.001	0.002	0.001	0.005	–	0.002	0.001	0.007	0.008	0.004	0.02	0.04	0.01
	DH9 5	cpx	9.5	0.24	2.0	0.5	3.7	1.7	0.7	0.5	2.9	3.9	1.0	2.7	2.1	0.33
	DH9 6	ol	29.1	0.002	0.010	0.002	0.01	–	0.002	0.001	0.01	0.01	0.01	0.02	0.04	0.01
	DH9 7	opx	19.4	0.001	0.014	0.004	0.04	0.02	0.02	0.02	0.11	0.25	0.08	0.3	0.40	0.08
Dish Hill 32	DH32 1	cpx	12.1	2.20	7.5	1.2	6	2.0	0.7	0.5	2.84	3.4	0.8	2.2	1.8	0.27
	DH32 2	opx	19.3	0.005	0.028	0.004	0.03	0.01	0.01	0.01	0.05	0.13	0.04	0.17	0.25	0.05
Dish Hill 18	DH 18 1	cpx	9.1	2.75	8.8	1.3	7.0	2.6	1.0	0.7	3.97	5.1	1.2	3.4	2.8	0.42
	DH18 2	ol	28.8	0.002	0.001	0.001	0.01	0.01	0.001	0.001	0.01	0.01	0.01	0.01	0.04	0.01
	DH18 3	opx	19.5	0.4	0.7	0.08	0.33	0.11	0.02	0.04	0.16	0.30	0.10	0.34	0.43	0.08
Dish Hill 6	DH6 4	cpx	9.2	1.9	5.4	0.8	4.9	1.9	0.7	0.5	3.0	3.9	1.0	2.8	2.2	0.34
	DH6 1	opx	19.3	0.2	0.4	0.04	0.16	0.05	0.01	0.02	0.10	0.20	0.07	0.27	0.39	0.08
	DH6 2	spinel	11.6	0.003	0.01	0.002	0.004	–	0.0002	0.0004	0.002	0.002	0.001	0.002	0.002	0.001

LA-ICP-MS data. opx = orthopyroxene, cpx = clinopyroxene, ol = olivine, sp = spinel.

were controlled by internal normalization [19] using ^{25}Mg. Accuracy was ensured by external calibration using standards glasses BCR2g and BHVO2g (reference concentrations taken from [20]). Finally, limit of detection for each analysis was estimated at 3 times the standard deviation of the background divided by the sensitivity of the instrument as monitored by ^{25}Mg.

4. Results

Fig. 2 shows the results of orthopyroxene and clinopyroxene pairs (olivine is also included) in 6 lherzolitic to harzburgitic peridotite xenoliths from Dish Hill. Primitive mantle-normalized clinopyroxene REE patterns are variable, containing flat REE, LREE depleted and LREE enriched signatures. Two Opx/Cpx (and at least 4 Ol/Cpx) pairs exhibit LREE disequilibrium as exemplified by deviations of the apparent LREE partition coefficients from the theoretical equilibrium line. Such disequilibria are most likely due to very recent introduction of a LREE-enriched contaminant, such as the host magma. Either some of these minerals have reacted locally with infiltrating fluids/melts or they contain LREE-bearing fluid inclusions along intragranular cracks Importantly, the fact that disequilibrium exists even when mineral cores are measured shows

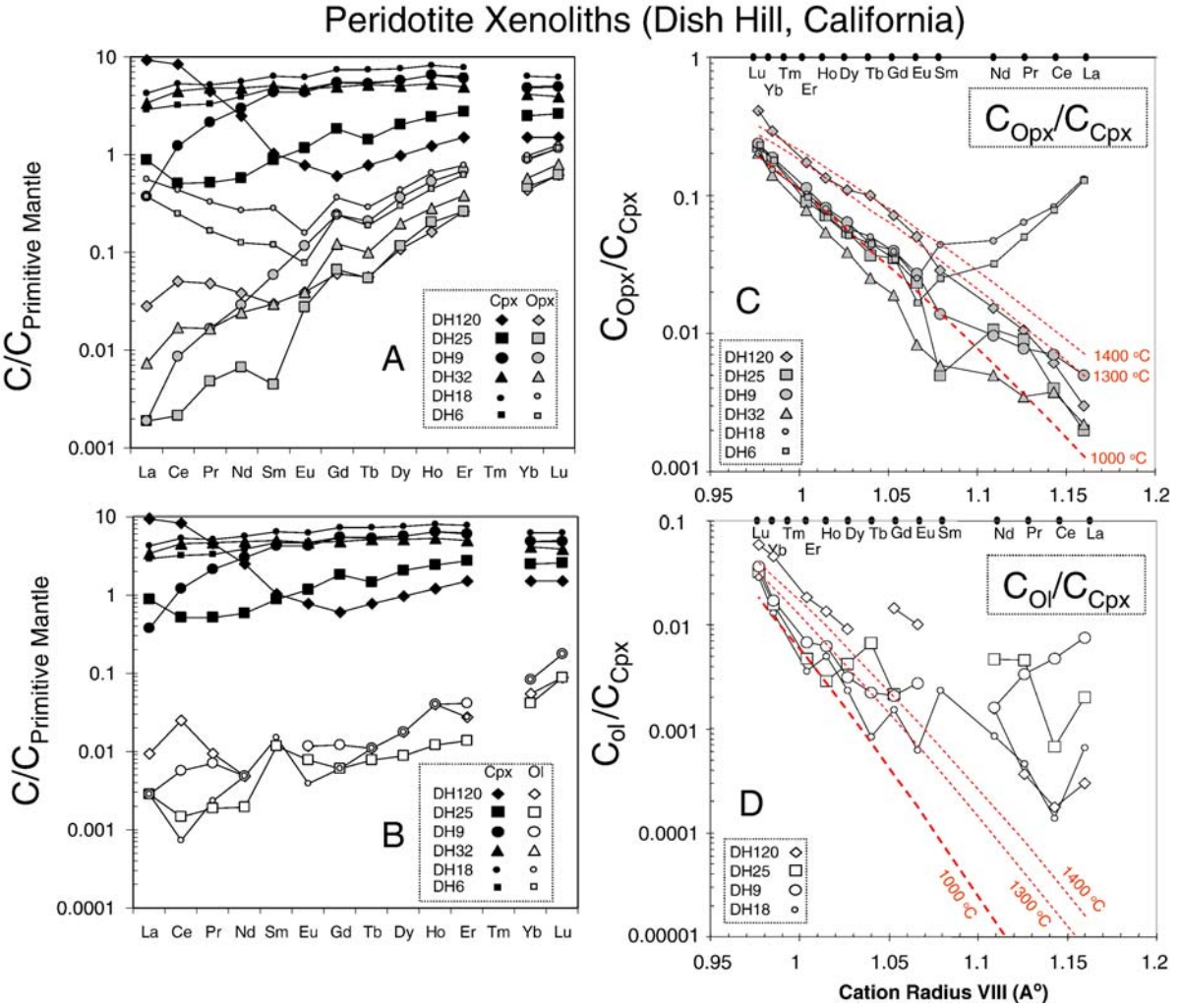

Fig. 2. Results of laser ablation ICP-MS measurements for six xenoliths from Dish Hill cinder cone in southern California, USA. A) Primitive mantle-normalized REE contents in Cpx and Opx. B) Primitive mantle-normalized REE contents in Ol and Cpx. Samples denoted by different symbol shapes as shown in the legend; colors correspond to specific mineral phases. C) and D) show apparent partitioning of REEs between Opx and Cpx and between Ol and Cpx plotted against VIII-fold cationic radius. Symbol shapes correspond to the same symbol shapes in A) and B). Dashed lines correspond to the equilibrium partitioning curves at different temperatures as shown in Fig. 1. (For interpretation of the references to colour in this figure legend, the reader is referred to the web version of this article.)

that, in some cases, no amount of mineral leaching will remove the effects of recent contamination. This underscores the extreme caution that must be taken when interpreting trace-element and isotopic compositions of clinopyroxene grains alone. Thus, analyzing Opx/Cpx pairs would at the very least provide a conservative filter for samples in disequilibrium.

The Gakkel Ridge abyssal peridotites [17] have clinopyroxenes characterized by extremely LREE-depleted, moderately LREE-depleted, and slightly LREE-enriched signatures (Fig. 3). Hellebrand et al. [17] suggested the LREE-depleted samples were formed by variable degrees of near-fractional melting, whereas the LREE-enriched samples were formed by melt infiltration into the lithosphere. Many of the Opx/Cpx pairs appear to be in LREE disequilibrium. Interestingly, the LREE-depleted samples are furthest from equilibrium while the LREE-enriched samples are closer to equilibrium. In other words, the more metasomatized samples appear to be closer in equilibrium.

5. Discussion

5.1. Xenoliths

Based on the above observations, we have confirmed the well-known fact that LREE-enrichment in mantle xenoliths is often a manifestation of host lava contamination or recent metasomatism by the pre-eruptive magmatic precursor [5,6,15]. Essentially, much of the apparent LREE-enrichments seen in xenoliths can be explained by the injection and subsequent freezing in of small amounts of melt. Our study provides a means of identifying when mineral pairs are in disequilibrium. We foresee it being a valuable tool in studies of very small xenoliths (e.g., cm-size) where interaction with the host magma might be greatest. However, being able to assess the degree of disequilibria could open up many new doors in the studies of mantle xenoliths because many basaltic magmas, upon closer examination, contain micro-xenoliths.

5.2. Abyssal peridotites

5.2.1. LREE-enriched peridotites

The abyssal peridotite data are more difficult to explain. Unlike the xenolith case study, the metasomatized abyssal peridotites appear to be more in equilibrium than those having clinopyroxenes with LREE-depleted signatures. One explanation is that secondary infiltration of small amounts of magmas not only precipitated tiny amounts of clinopyroxene but also facilitated trace element equilibration by rapid diffusional exchange through thin films of melt distributed along interconnected grain boundaries. An approach to equilibrium would be further facilitated if melt infiltration was associated with prolonged porous flow (e.g. [21,22]) as opposed to the brief injection and freezing in of the host lava in the case of mantle xenoliths. We thus speculate that the more protracted timescales and larger integrated melt/rock ratios associated with porous flow allows for trace-element re-equilibration and LREE-

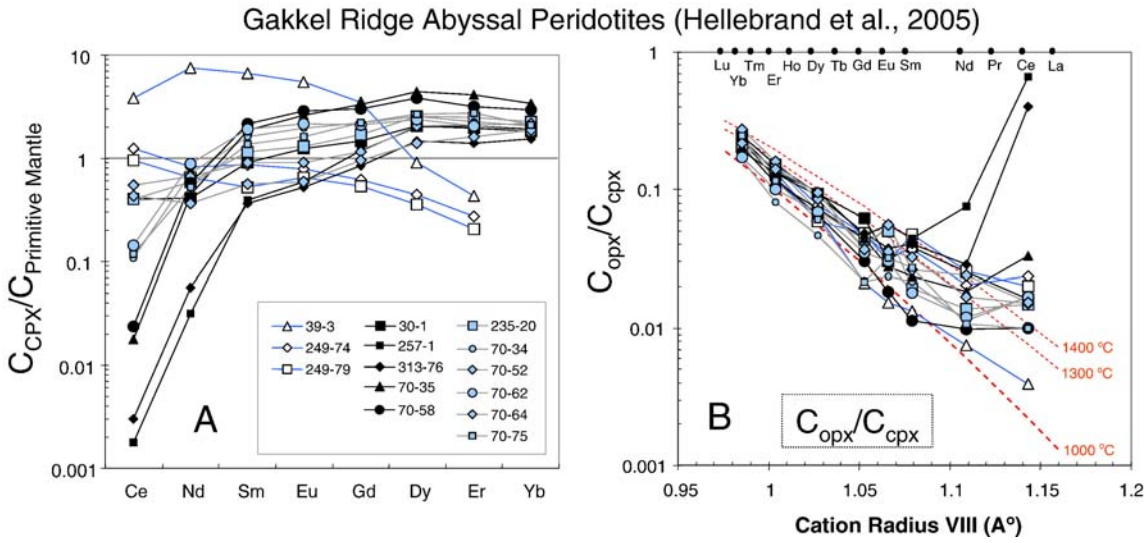

Fig. 3. Orthopyroxene and clinopyroxene REE data from the Gakkel ridge abyssal peridotites [17]; olivine data were not available. A) Primitive-mantle normalized REE contents in Cpx. B) Same format as in Fig. 2c and d. Symbols as in 3A.

enrichment whereas the short timescales and low integrated melt/rock ratios associated with melt infiltration in mantle xenoliths probably limits diffusive exchange between minerals and melt. We speculate that the LREE-enriched abyssal peridotites may have derived from the deeper (and hence hotter) parts of the lithospheric mantle, where melts and fluids rising up through porous flow have much longer to equilibrate with the lithospheric mantle.

5.2.2. LREE-depleted peridotites

We now address the disequilibrium seen in the LREE-depleted abyssal peridotites. One possibility may be elemental fractionations caused by differential solid-state diffusion rates of the REEs during *subsolidus cooling*. At higher temperatures, orthopyroxene can hold more REEs and the proportional effect is greatest in LREEs; this effect is shown in Figs. 1 and 3. The diffusivities of HREEs are at least an order of magnitude higher than that of LREEs and therefore one might expect that HREEs would be equilibrated sooner than the LREEs during cooling [7]. Such a process could in theory produce apparent U-shaped $D_i^{opx/cpx}$ versus cationic radii patterns. However, the magnitudes of the deviations of $D_i^{opx/cpx}$ from equilibrium in some samples are likely too large to be explained solely by differential diffusive exchange during cooling. For example, some samples (257-1 and 313-76) have LREE Opx/Cpx ratios too high to be explained by any reasonable initial temperatures. These samples, despite their overall LREE-depleted signatures, must still have experienced some re-enrichment in LREEs (enough to affect the Opx more than the Cpx) yet unlike the LREE-enriched peridotites, mineral–mineral equilibrium was not re-established.

A better explanation for disequilibria in the LREE-depleted harzburgites might be that such peridotites experienced only limited amounts of melt infiltration unlike that proposed for the LREE-enriched abyssal peridotites above. Perhaps the LREE-depleted peridotites derive from the cold part of the lithospheric mantle, where any infiltrating melts quickly freeze in, thereby preventing re-equilibration. To place this in context, we can consider some back-of-the-envelope calculations. Using the clinopyroxene diffusion data of [7,23] as a guide, it would take only ~ 15,000 years for a pyroxene having a 1 mm radius to fully equilibrate in terms of Yb at lithospheric mantle temperatures (diffusivity of Yb at 1200 °C is $\sim 5\times10^{-19}$ m^2/s). For the same mineral grain, differences in re-equilibration times for two elements having different diffusivities follow $t_1/t_2 = d_2/d_1$, where t is time and d is diffusivity. For La, which has a diffusivity of $\sim 2\times10^{-20}$ at 1200 °C, we find that $t_{La}/t_{Yb} \sim 25$, which means that it takes 25 times longer for La to re-equilibrate than Yb (~ 400,000 years). If we had used cooler temperatures, the lag time in equilibration would have been even longer.

6. Conclusions

A framework for quantifying REE disequilibria between mineral phases in the subsolidus state was presented here and its utility demonstrated in peridotite xenoliths and abyssal peridotites. We confirm the well-known fact that mantle xenoliths often suffer from recent metasomatic or contamination effects, but that their pre-eruptive REE signatures can be determined by filtering out those in disequilibrium using the simple test presented here. We also showed that most of the investigated abyssal peridotites are not in LREE equilibrium, but the extent of disequilibrium and its relation to the overall metasomatic signature may shed light on the origin of abyssal peridotites. Our study shows that coupling such studies with detailed isotopic studies and petrography are necessary and will surely be rewarding, possibly leading to a better understanding of the origin and chemical evolution of continental and oceanic lithospheric mantle. We remark that the approach taken here for REEs can be modified to deal with other minerals not necessarily confined to ultramafic compositions. Our model can also in theory be extended to monovalent alkali Earth elements (Li, Na, K, Rb, Cs), provided these elements can be accurately measured by in situ analytical techniques.

Acknowledgments

This work was supported by NSF grants (EAR 0549268, 0440033, 0309121) and a Packard Fellowship to Lee. We thank P. Luffi, A. Harbert, W. P. Leeman, R. Rudnick, J. Snow, and E. Hellebrand for the discussions. We are grateful for the constructive reviews by Y. Liang and an anonymous reviewer.

References

[1] F. Albarede, P. Telouk, J. Blichert-Toft, M. Boyet, A. Agranier, B. Nelson, Precise and accurate isotopic measurements using multiple-collector ICPMS, Geochim. Cosmochim. Acta 68 (2004) 2725–2744.

[2] S.B. Mukasa, H.G. Wilshire, Isotopic and trace element compositions of upper mantle and lower crustal xenoliths, Cima volcanic field, California: implications for evolution of the subcontinental lithospheric mantle, J. Geophys. Res. 102 (1997) 20,133–120,148.

[3] W.L. Griffin, N.J. Pearson, E. Belousova, S.E. Jackson, E. van Achterbergh, S.Y. O'Reilly, S.R. Shee, The Hf isotope composition of cratonic mantle: LAM-MC-ICPMS analysis of zircon megacrysts in kimberlites, Geochim. Cosmochim. Acta 64 (2000) 133–147.
[4] N.J. Pearson, O. Alard, W.L. Griffin, S.E. Jackson, S.Y. O'Reilly, In situ measurement of Re–Os isotopes in mantle sulfides by laser ablation multicollector-inductively coupled plasma mass spectrometry: analytical methods and preliminary results, Geochim. Cosmochim. Acta 66 (2002) 1037–1050.
[5] A. Zindler, E. Jagoutz, Mantle cryptology, Geochim. Cosmochim. Acta 52 (1988) 319–333.
[6] H.G. Stosch, Rare earth element partitioning between minerals from spinel peridotite xenoliths, Contrib. Mineral. Petrol. 78 (1982) 166–174.
[7] J.A. Van Orman, T.L. Grove, N. Shimizu, Rare earth element diffusion in diopside: influence of temperature, pressure, and ionic radius, and an elastic model for diffusion in silicates, Contrib. Mineral. Petrol. 141 (2001) 687–703.
[8] S.M. Eggins, R.L. Rudnick, W.F. McDonough, The composition of peridotites and their minerals: a laser-ablation ICP-MS study, Earth Planet. Sci. Lett. 154 (1998) 53–71.
[9] C.-T.A. Lee, A. Harbert, W.P. Leeman, Extension of lattice strain theory to mineral/mineral rare-earth element partitioning: an approach for assessing disequilibrium and developing internally consistent partition coefficients between olivine, orthopyroxene, clinopyroxene, and basaltic melt, Geochim. Cosmochim. Acta 71 (2007) 481–496, doi:10.1016/j.gca.2006.1009.1014.
[10] J. Blundy, B. Wood, Prediction of crystal-melt partition-coefficients from elastic-moduli, Nature 372 (1994) 452–454.
[11] J.H. Bedard, Partitioning coefficients between olivine and silicate melts, Lithos 83 (2005) 394–419.
[12] G. Witt-Eickschen, H.S. O'Neill, The effect of temperature on the equilibrium distribution of trace elements between clinopyroxene, orthopyroxene, olivine and spinel in upper mantle peridotite, Chem. Geol. 221 (2005) 65–101.
[13] B.J. Wood, J.D. Blundy, Trace element partitioning under crustal and uppermost mantle conditions: the influences of ionic radius, cation charge, pressure, and temperature, Treatise Geochem. 2 (2003) 395–424.
[14] D. Canil, Mildly incompatible elements in peridotites and the origins of mantle lithosphere, Lithos 77 (2004) 375–393.
[15] G. Witt-Eickschen, H.S.C. O'Neill, The effect of temperature on the equilibrium distribution of trace elements between clinopyroxene, orthopyroxene, olivine and spinel in upper mantle peridotite, Chem. Geol. 221 (2005) 65–101.
[16] C.-T. Lee, The origin, evolution, and demise of continental lithospheric mantle: perspectives from Re–Os isotopes, geochemistry, petrology, and modeling, Harvard University, PhD Thesis, (2001).
[17] E. Hellebrand, J.E. Snow, S. Mostefaoui, P. Hoppe, Trace element distribution between orthopyroxene and clinopyroxene in peridotites from the Gakkel Ridge: a SIMS and NanoSIMS study, Contrib. Mineral. Petrol. 150 (2005) 486–504.
[18] C.T. Lee, R.L. Rudnick, W.F. McDonough, I. Horn, Petrologic and geochemical investigation of carbonates in peridotite xenoliths from northeastern Tanzania, Contrib. Mineral. Petrol. 139 (2000) 470–484.
[19] H.P. Longerich, D. Gunther, S.E. Jackson, Elemental fractionation in laser ablation inductively coupled plasma mass spectrometry, Fresenius' J. Anal. Chem. 355 (1996) 538–542.
[20] S. Gao, X.M. Liu, H.L. Yuan, B. Hattendorf, D. Gunther, L. Chen, S.H. Hu, Determination of forty two major and trace elements in USGS and NIST SRM glasses by laser ablation-inductively coupled plasma-mass spectrometry, Geostand. Newsl. — J. Geostand. Geoanal. 26 (2002) 181–196.
[21] O. Navon, E. Stolper, Geochemical consequences of melt percolation — the upper mantle as a chromatographic column, J. Geol. 95 (1987) 285–307.
[22] J.L. Bodinier, G. Vasseur, J. Vernieres, C. Dupuy, J. Fabries, Mechanism of mantle metasomatism: geochemical evidence from the Lherz orogenic peridotite, J. Petrol. 31 (1990) 597–628.
[23] D.J. Cherniak, Y. Liang, Rare earth element diffusion in natural enstatite, Geochim. Cosmochim. Acta 71 (2007) 1324–1340.